PROCEEDINGS OF SCIENCE

A CORSIKA study on the influence of muon detector thresholds on the separability of primary cosmic rays at highest energies

Sarah Müller* **and Markus Roth**
Institut für Kernphysik, Karlsruhe Institute of Technology (KIT), Karlsruhe, Germany
E-mail: sarah.mueller2@kit.edu, markus.roth@kit.edu

The precise determination of the number of muons in extensive air showers is a key issue for being able to separate showers that have been initiated by different primary particles. In the context of planned muon detector extensions of the Pierre Auger and Telescope Array Observatories, we analyze CORSIKA shower simulations at energies above 10^{18} eV to quantify expectations on the separability of primary particles. We observe that an improved separation power, described in terms of the figure of merit, is achieved if muons of low momenta are rejected, i.e. the detector energy threshold is set to ~ 1 GeV. Investigating the impact of photonuclear reactions in the shower development, we find that there are less muons produced by photonuclear precursor reactions in iron initiated showers than in proton initiated showers. At low momenta, these muons considerably lower the figure of merit and hence worsen the discrimination of primary masses.

The 34th International Cosmic Ray Conference,
30 July - 6 August, 2015
The Hague, The Netherlands

*Speaker.

PoS(ICRC2015)419

1. Introduction

The determination of the number of muons in extensive air showers allows the separation of different mass groups of primaries at ultra-high energies. Knowledge of the muonic shower component on an event-by-event basis makes it possible to derive composition-discriminated fluxes in the range from about 10^{18} eV up to the highest energies. This allows for carrying out composition-enhanced anisotropy searches based on event-by-event estimates of the primary mass, to search for GZK secondaries and ultra-high energy photons produced in the astrophysical environment of sources, and to test our understanding of hadronic interactions at center of mass energies around and above 60 TeV.

Important results on the composition of cosmic rays by means of muon detection techniques have been obtained by the Haverah Park [1, 2, 3], Yakutsk [4, 5, 6] and AGASA experiments [7, 8, 9] and more recently by the KASCADE [10, 11, 12] and KASCADE-Grande [13, 14] experiments. Currently, the Pierre Auger [15, 16] and the Telescope Array collaborations [17] are planning to extend their experiments by muon detectors to get an additional important shower observable for composition analyses of ultra-high-energy cosmic rays.

For the design of future muon detectors, it is essential to quantify expectations on the separability of primary particles. The detector properties have to be chosen in a way to optimize the performance and to extract an unbiased estimate of the number of muons with smallest possible statistical and systematic uncertainties to ensure the largest separation power possible.

In this work, we simulate proton and iron initiated showers at an energy of $3.16 \cdot 10^{18}$ eV. We quantify the separation power between showers that have been initiated by different primary particles by means of the figure of merit. For different muon detection energy thresholds, we study the figure of merit and investigate the influence of photonuclear reactions preceding the production of muons. We find that muons from photonuclear reactions lower the figure of merit and hence do not contribute to the separation of primary particles. As a result, we recommend energy thresholds of at least 1 GeV for future muon detectors.

2. Energy threshold dependence of f_{FoM}

In our analysis, we use the CORSIKA (COsmic Ray SImulations for KAscade) software [18] which has been designed for detailed simulations of extensive air showers initiated by high energy cosmic ray particles. For the treatment of hadronic interactions at lower energies, we employ the FLUKA model [19], at high energies we choose the EPOS-LHC model [20, 21]. The zenith angle of the primary particle is set to $\theta = 38^{\circ}$ while the azimuth angle φ is generated randomly. We simulated 115 unthinned showers with primary energy of $3.16 \cdot 10^{18}$ eV for proton and iron primary cosmic ray particles, respectively. Information on the interactions preceding the decay into muons is made available by the EHISTORY [22] option.

Since a detector of finite size A samples a finite amount of muons, the uncertainty in the muon number estimate is not only governed by shower-to-shower fluctuations, but is also driven by the sheer number of muons collected in a limited area. To mimic an ideal detector, we consider a ring in the shower plane with the shower core as its center. The inner and outer radii, corresponding to the distances from the shower axis in the shower plane, are given by r and $r + \delta r$, respectively. We

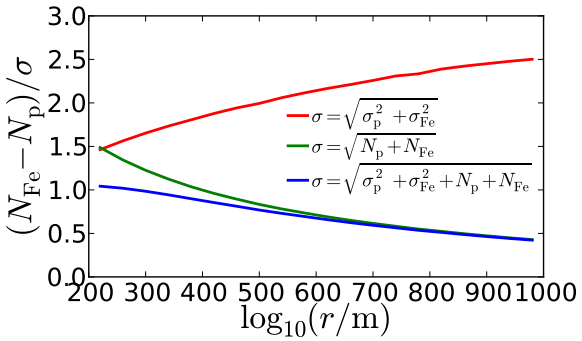

Figure 1: Impact of shower-to-shower fluctuations and Poissonian uncertainties on the figure of merit f_FoM for muon energies $E_\mu \geq 1\,\mathrm{GeV}$, and a detection area $A = 10\,\mathrm{m}^2$.

have chosen δr such that the influence of the steeply falling lateral distribution is hardly changing the muon density within the ring. We determine the number of muons N_ring in the ring for each simulated air shower, assuming no significant azimuthal asymmetries being present. The expected number of muons, $\hat{N}$, in a sampling area A is hence given by $\hat{N} = N_\mathrm{ring}\frac{1}{\pi}\frac{A}{(r+\delta r)^2-r^2}$.

The *figure of merit* is used to quantify the separation power

$$f_\mathrm{FoM} = \frac{N_\mathrm{Fe}-N_\mathrm{p}}{\sqrt{\sigma_\mathrm{p}^2+\sigma_\mathrm{Fe}^2+N_\mathrm{p}+N_\mathrm{Fe}}} \tag{2.1}$$

between showers that have been induced by a primary proton or iron nucleus. We account for uncertainties resulting from shower-to-shower fluctuations by the standard deviations σ_j with $j \in \{\mathrm{p}, \mathrm{Fe}\}$. Uncertainties due to the finite sampling are parametrized by the Poissonian uncertainties $\sigma_j^\mathrm{Poisson} = \sqrt{N_j}$, where N_j corresponds to the mean of the muon numbers $\hat{N}$ averaged over the set of shower simulations for a given primary. The different contributions are displayed explicitly in Fig. 1. For the considered primary energy of $3.16 \cdot 10^{18}\,\mathrm{eV}$, the total fluctuations are driven by shower-to-shower fluctuations below distances of about 200 m, while Poissonian fluctuations dominate more and more with increasing distance to the shower core.

In order to quantify expectations on the influence of detector energy thresholds on the figure of merit, we impose muon energy thresholds of 0.1, 1, and 2 GeV in the analysis presented here. For the purpose of reducing computational costs, we do not simulate muons stemming from reactions with energy $\leq 0.1\,\mathrm{GeV}$. The resulting lateral distributions (Fig. 2 left for proton) are used furthermore to derive a quantitative measure for composition studies. At radii up to about 400 m, an ascending ordering of f_FoM with increasing muon threshold becomes apparent (Fig. 2 right), i.e. the higher the muon threshold the larger the figure of merit. A turnover can be observed at larger distances from the shower core due to the increasing impact of Poisson statistics in this radial range. For a better understanding of the improved separation power for larger thresholds close to the core, we inspect the influence of photonuclear reactions on the figure of merit in the next section.

3. Impact of photonuclear reactions

An air shower initiated by a nucleus with atomic number A can be considered as a superposition of A nucleon induced air showers [23]. Due to the reduced energy of each of these nucleon

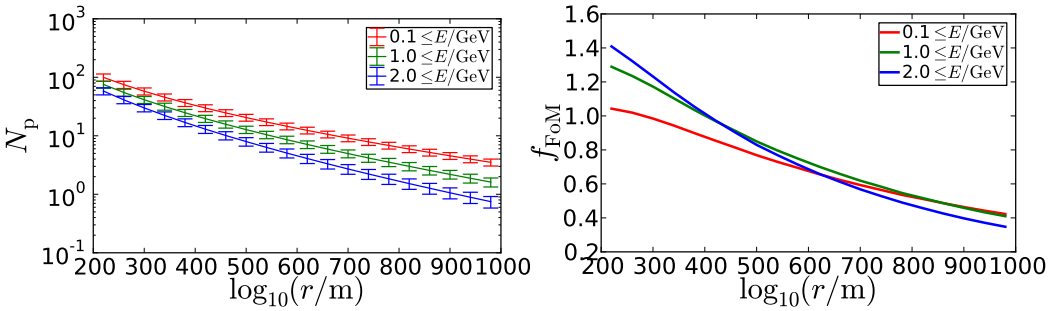

Figure 2: Lateral density distribution for proton induced showers with error bars denoting one standard deviation due to shower-to-shower fluctuations (left) and figure of merit (right) for muon energy thresholds of 0.1, 1, and 2 GeV, and a detection area $A = 10\,\mathrm{m}^2$.

showers, less interaction generations and hence a reduced loss of energy in electromagnetic interactions is predicted. As a consequence, a shower caused by such a nucleus is expected to exhibit an increased number of muons, from the hadronic part of the shower, compared to a proton initiated shower with the same primary energy. On the other hand, since we expect less electromagnetic interactions in showers initiated by nuclei, a reduced number of muons resulting from photonuclear reactions would be the consequence. Observing a worsening of the figure of merit with decreasing muon energy threshold (cf. Section 2), it is hence worth to investigate the energy dependent impact of muons from photonuclear reactions on the separability of primary particles.

The EHISTORY [22] option of the simulation software CORSIKA [18] gives additional information on the precursors of all muons. We employ the provided hadronic generation counter to tag photonuclear reactions of the type $\gamma + \mathrm{air} \longrightarrow \{\mathrm{hadron} + X\}$ or $\{\rho^0$ or $\omega^0\,(+\mathrm{recoil\ nucleus})\}$ as well as $\mu^+\mu^-$ pair creation processes $\gamma + \mathrm{air} \longrightarrow \mu^+\mu^-$ that have been undergone by precursors of the muons arriving at ground. In this manner, we can separate muons originating from photonuclear reactions from those which did not have any interference with photons from the air shower.

We find that only a fraction of $6-11\%$ of the muons arriving at ground originate from preceding photonuclear reactions. Muon energy distributions for both iron and proton primaries are shown in Fig. 3. The energy distribution at $r = 918 \pm 82\,\mathrm{m}$ is shifted to lower energies compared to the distribution at $r = 220 \pm 20\,\mathrm{m}$. At the lowest energies, spectra of proton and iron primaries hardly differ for muons without photonuclear precursors ($i = \Sigma - \gamma$). Even though muons originating from photonuclear processes ($i = \gamma$) are highly suppressed with respect to muons from other hadronic interaction processes ($i = \Sigma - \gamma$), their distributions approach each other at low muon energies. Therefore, we separately inspect the influence of these muons on the different components of the figure of merit (2.1), i.e. its nominator and denominator, in the low energy region.

For a muon energy threshold E_{th}, the nominator of (2.1) is given by $\int_{E_{\mathrm{th}}}^{\infty} \mathrm{d}\Delta N^i = \int_{E_{\mathrm{th}}}^{\infty} \mathrm{d}\left(N^i_{\mathrm{Fe}} - N^i_{\mathrm{p}}\right)$, where $i = \gamma, \Sigma-\gamma, \Sigma$ denote the parts of muons with preceding photonuclear reactions only, without photonuclear reactions, and the sum of both contributions (i.e. all muons), respectively. $\int_{E_{\mathrm{th}}}^{\infty} \mathrm{d}\Delta N^\gamma$, shown in Fig. 4, is negative for muon energy thresholds up to 9.8 GeV for $r = 220 \pm 20\,\mathrm{m}$ and 1.4 GeV for $r = 918 \pm 82\,\mathrm{m}$, i.e. the mean number $\int_{E_{\mathrm{th}}}^{\infty} \mathrm{d}N_{\mathrm{Fe}}$ of muons from iron initiated showers is smaller than $\int_{E_{\mathrm{th}}}^{\infty} \mathrm{d}N_{\mathrm{p}}$ for proton initiated showers in contrast to the situation for muons without preceding photonuclear reactions. Hence, photonuclear reactions generally lower the nominator of

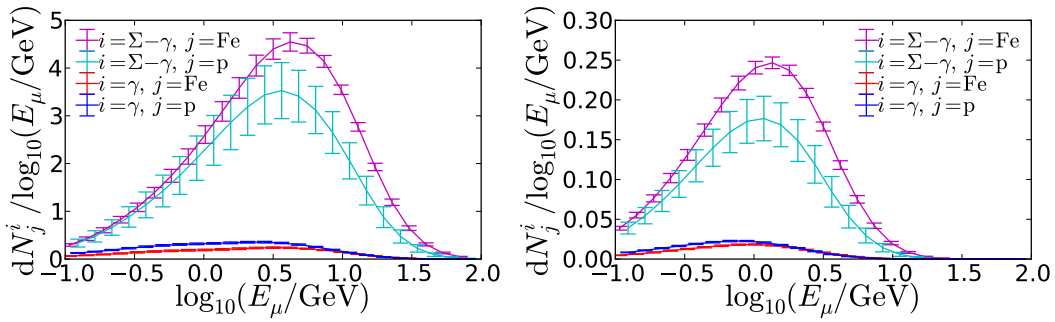

Figure 3: Muon energy distributions for Fe and p primaries at distances $r = 220 \pm 20\,\mathrm{m}$ (left) and $r = 918 \pm 82\,\mathrm{m}$ (right). Muon numbers are averaged and normalized to a sampling area $A = 10\,\mathrm{m}^2$, error bars denote one standard deviation due to shower-to-shower fluctuations. Results are shown for muons with only ($i = \gamma$) and without ($i = \Sigma - \gamma$) preceding photonuclear reactions.

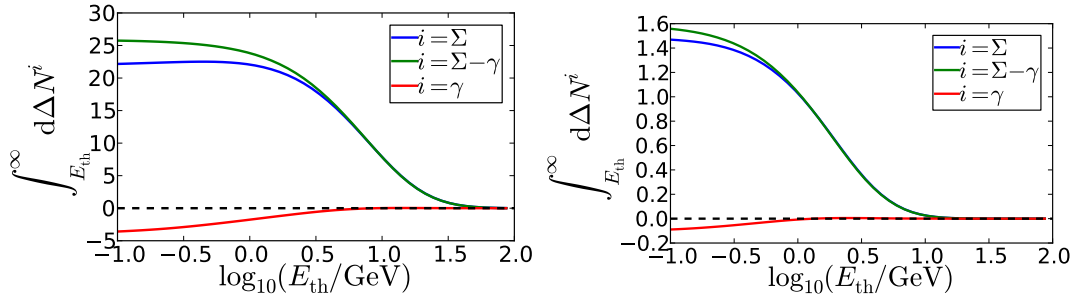

Figure 4: Muon number difference $\int_{E_\mathrm{th}}^{\infty} \mathrm{d}\Delta N^i = \int_{E_\mathrm{th}}^{\infty} \mathrm{d}\left(N^i_\mathrm{Fe} - N^i_\mathrm{p}\right)$ for muon energy thresholds E_th in bins of muon energy at distance $r = 220 \pm 20\,\mathrm{m}$ (left) and $r = 918 \pm 82\,\mathrm{m}$ (right) from the shower core. The superscripts $i = \gamma, \Sigma - \gamma, \Sigma$ denote the parts of muons with preceding photonuclear reactions only, without photonuclear reactions, and the sum of both contributions, respectively.

the total figure of merit up to these energy thresholds. For increasing muon energy thresholds the effect of muons from photonuclear reactions becomes more and more insignificant.

In addition to the sheer muon number difference $\int_{E_\mathrm{th}}^{\infty} \mathrm{d}\Delta N^i$, the occurring uncertainties due to shower-to-shower fluctuations and Poisson statistics limit the figure of merit. The dependence of the uncertainties $\int_{E_\mathrm{th}}^{\infty} \mathrm{d}\,\sigma^i$ due to shower-to-shower fluctuations and Poissonian uncertainties on the imposed muon energy threshold is depicted in Fig. 5 for distances $r = 220 \pm 20\,\mathrm{m}$ and $r = 918 \pm 82\,\mathrm{m}$ from the shower core. The uncertainties, and hence the denominator of the figure of merit (2.1), are slightly smaller for muons without preceding photonuclear reactions ($i = \Sigma - \gamma$) than for the all muon case ($i = \Sigma$). However, the splitting is less pronounced compared to the splitting in the muon number difference.

The increase of the nominator $\int_{E_\mathrm{th}}^{\infty} \mathrm{d}\Delta N^{\Sigma-\gamma}$ together with a lowered denominator $\int_{E_\mathrm{th}}^{\infty} \mathrm{d}\,\sigma^{\Sigma-\gamma}$ w.r.t. the all muon case ($i = \Sigma$) leads to a splitting in the figure of merits $\int_{E_\mathrm{th}}^{\infty} \mathrm{d}\, f_\mathrm{FoM}^{\Sigma-\gamma}$ and $\int_{E_\mathrm{th}}^{\infty} \mathrm{d}\, f_\mathrm{FoM}^{\Sigma}$ shown in Fig. 6 up to a radius dependent threshold E_th. For $r = 220 \pm 20\,\mathrm{m}$ and $r = 918 \pm 82\,\mathrm{m}$, these energy thresholds are at about 10.5 GeV and 1.5 GeV, respectively. Note that the maximal figure of merit $\int_{E_\mathrm{th}}^{\infty} \mathrm{d}\, f_\mathrm{FoM}^{\Sigma}$ of all muons is by a factor of about 2.5 higher at $r = 220 \pm 20\,\mathrm{m}$ than at

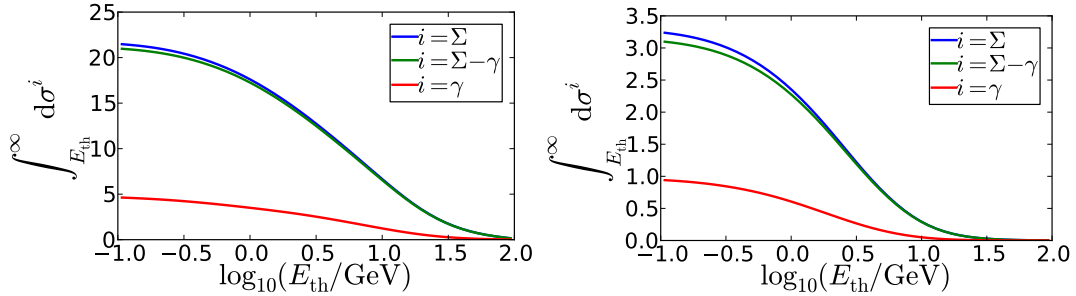

Figure 5: Uncertainties $\int_{E_{\rm th}}^{\infty} {\rm d}\,\sigma^i$ due to shower-to-shower fluctuations and Poissonian uncertainties for muon energy thresholds $E_{\rm th}$ at $r = 220 \pm 20\,{\rm m}$ (left) and $r = 918 \pm 82\,{\rm m}$ (right) from the shower core. The superscripts $i = \gamma, \Sigma - \gamma, \Sigma$ denote the uncertainties for muons with preceding photonuclear reactions only, without photonuclear reactions, or both contributions, respectively.

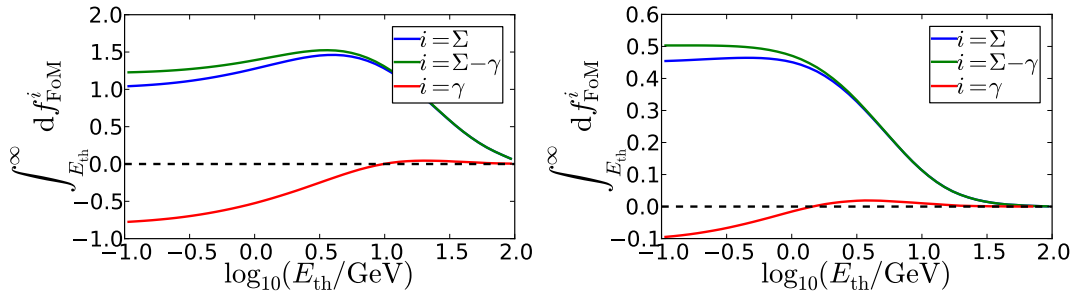

Figure 6: Figure of merit $\int_{E_{\rm th}}^{\infty} {\rm d}\,f^i_{\rm FoM}$ for muon energy thresholds $E_{\rm th}$ at $r = 220 \pm 20\,{\rm m}$ (left) and $r = 918 \pm 82\,{\rm m}$ (right) from the shower core and detection area $A = 10\,{\rm m}^2$. The superscripts $i = \gamma, \Sigma - \gamma, \Sigma$ denote the figure of merit for muons with preceding photonuclear reactions only, without photonuclear reactions, or both contributions, respectively.

$r = 918 \pm 82\,{\rm m}$. In conclusion, muons from photonuclear reactions in fact produce a lowering of the figure of merit. However, the increase of $\int_{E_{\rm th}}^{\infty} {\rm d}\,f^i_{\rm FoM}$ up to an optimal energy threshold occurs irrespective of the fact if muons from photonuclear reactions are accounted for or not.

4. Estimate of optimal muon detector energy thresholds

We quantify the radius dependent optimal range of muon energy thresholds in Fig. 7 left for both cases $i = \Sigma$ and $i = \Sigma - \gamma$. The muon energy thresholds $E_{\rm th}^{f^i_{\rm FoM,max}}$ where the figures of merit are maximal are plotted and the energy threshold regions where the corresponding figures of merit are larger or equal than 95% of $f^i_{\rm FoM,max}$ are displayed by error bars. The optimal energy thresholds depend on the required radial range. They are slightly smaller for the scenario of no muons from photonuclear reactions than for the all muon case. For future muon detector experiments with a radial range up to 800 m, a threshold of about 1 GeV would be best suited for the considered primary energy of $3.16 \cdot 10^{18}\,{\rm eV}$, while for radial ranges up to 550 m only, $E_{\rm th} \sim 2\,{\rm GeV}$ yields better figure of merits. However, a muon energy detector threshold of about 1 GeV would still produce a figure of merit deviating at most 5% from the optimal value.

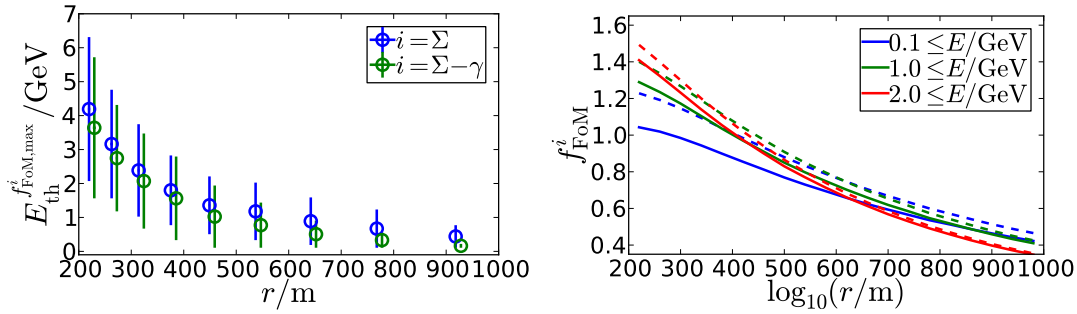

Figure 7: Left: Radius dependent optimal muon energy thresholds, error bars display the energy threshold region where the corresponding figure of merit is larger or equal than 95% of $f^i_{\mathrm{FoM,max}}$. Right: Lateral dependence of the figure of merit if muons with preceding photonuclear reactions are included (solid curves) or excluded (dashed curves) for different muon energy thresholds of 0.1 GeV, 1 GeV, and 2 GeV and a detection area $A = 10\,\mathrm{m}^2$.

The radial dependence of the figure of merit for the muon energy thresholds of 1 and 2 GeV in comparison to a threshold of 0.1 GeV is shown in Fig. 7 right. In addition to the results from Fig. 2 right, the figure of merit is not only displayed for the all muon case but also for the scenario where muons from photonuclear reactions are excluded. The figure of merit is most affected by the influence of muons with preceding photonuclear reactions for the lowest threshold of 0.1 GeV, as seen before in Figs. 4 to 6. For higher thresholds of 1 and 2 GeV shown here, the separation between the figure of merits for muons with and without preceding photonuclear reactions becomes increasingly smaller. However, although photonuclear reactions do lower the figure of merit, the ascending ordering of the figure of merit with increasing muon energy threshold from 0.1 GeV to 2 GeV up to about 400 m remains if muons from photonuclear reactions are excluded. At about 450 m, the 1 GeV and 2 GeV curves intersect in the all muon case, such that better figure of merits are yielded for an energy threshold of 2 GeV. However, Poisson statistics leads to a rapid decrease of the figure of merit for large distances to the shower core, indicating small discrimination abilities irrespective of the muon energy threshold.

5. Conclusion

In this work, we address the statistical significance of composition measurements, recording muons on a limited sampling area A, w.r.t. the applied muon energy detector thresholds. We find that muons stemming from photonuclear precursor reactions lower the figure of merit. However, an ascending ordering of the figure of merit with increasing muon energy threshold from 0.1 GeV to 2 GeV up to about 400 m for a primary energy of $3.16 \cdot 10^{18}$ eV even remains if muons from photonuclear reactions are excluded.

We quantify the radius dependent optimal muon energy threshold ranges where the corresponding figures of merit are at least 95% of the maximal value. For future muon detectors with radial ranges up to 550 m, a threshold of about 2 GeV would be best suited. At higher distances to the shower core, Poisson statistics leads to a rapid decrease of the figure of merit, indicating small discrimination abilities irrespective of the muon energy threshold. However, a muon energy

detector threshold of about 1 GeV, yielding slightly better figures of merit beyond 550 m, would deviate at most 5% from the optimal figures of merit in the $r \leq 550\,\mathrm{m}$ region.

Acknowledgments

This work is supported in part by the Helmholtz Alliance for Astroparticle Physics HAP, which is funded by the Initiative and Networking Fund of the Helmholtz Association.

References

[1] M. A. Lawrence, R. J. O. Reid, and A. A. Watson, *The cosmic ray energy spectrum above* 4×10^{17} eV *as measured by the Haverah Park array*, *J. Phys. G: Nucl. Part. Phys.* **17** (1991) 733.

[2] M. Ave, J. Knapp, J. Lloyd-Evans, M. Marchesini, and A. A. Watson, *The energy spectrum of cosmic rays in the range* $3 \times 10^{17}\,\mathrm{eV} - 4 \times 10^{18}\,\mathrm{eV}$ *as measured with the Haverah Park array*, *Astropart. Phys.* **19** (2003) 47–60.

[3] M. Ave, L. Cazón, J. A. Hinton, J. Knapp, J. Lloyd-Evans, and A. A. Watson, *Mass composition of cosmic rays in the range* $2 \times 10^{17}\,\mathrm{eV} - 3 \times 10^{18}\,\mathrm{eV}$ *measured with the Haverah Park array*, *Astropart. Phys.* **19** (2003) 61–75.

[4] I. Anatoly, *The Yakutsk array experiment: Main results and future directions*, *EPJ Web Conf.* **53** (2013) 04003.

[5] S. P. Knurenko, V. A. Kolosov, I. T. Makarov, Ye, V. R. Sleptsova, and G. G. Struchkov, *Muons with* $E_{\mathrm{th}} \geq 1\,\mathrm{GeV}$ *and mass composition in the energy range* $10^{18} - 10^{20}$ eV *observed by Yakutsk EAS array*, *Int. J. Mod. Phys. A* **20** (2005) 6900–6902.

[6] S. P. Knurenko and A. Sabourov, *Study of cosmic rays at the Yakutsk EAS array: energy spectrum and mass composition*, *Nucl. Phys. B - Proc. Suppl.* **212-213** (2011) 241–251.

[7] N. Chiba et al., *Akeno Giant Air Shower Array (AGASA) covering* $100\,\mathrm{km}^2$ *area*, *Nucl. Instrum. Meth. A* **311** (1992) 338–349.

[8] N. Hayashida et al., *Muons (*$\geq 1\,\mathrm{GeV}$*) in large extensive air showers of energies between* $10^{16.5}$ eV *and* $10^{19.5}$ eV *observed at Akeno*, *J. Phys. G: Nucl. Part. Phys.* **21** (1995) 1101.

[9] K. Shinozaki, *AGASA results*, *Nucl. Phys. B - Proc. Suppl.* **151** (2006) 3–10.

[10] T. Antoni et al., *The cosmic-ray experiment KASCADE*, *Nucl. Instrum. Meth. A* **513** (2003) 490–510.

[11] T. Antoni et al., *Muon density measurements with the KASCADE central detector*, *Astropart. Phys.* **16** (2002) 373–386.

[12] T. Antoni et al., *KASCADE measurements of energy spectra for elemental groups of cosmic rays: Results and open problems*, *Astropart. Phys.* **24** (2005) 1–25, [astro-ph/0505413].

[13] W. D. Apel et al., *The KASCADE-Grande experiment*, *Nucl. Instrum. Meth. A* **620** (2010) 202–216.

[14] W. D. Apel et al., *Kneelike Structure in the Spectrum of the Heavy Component of Cosmic Rays Observed with KASCADE-Grande*, *Phys. Rev. Lett.* **107** (2011).

[15] The Pierre Auger Collaboration, *Upgrade of the Pierre Auger Observatory*, *Proc. 34th ICRC, these proceedings* (2015).

[16] The Pierre Auger Collaboration, *Muons in air showers at the Pierre Auger Observatory: Mean number in highly inclined events*, *Phys. Rev. D* **91** (2015) [arXiv:1408.1421].

[17] The Telescope Array Collaboration, *Telescope Array Introduction*, *Proc. 33rd ICRC* (2013).

[18] D. Heck, J. Knapp, J. N. Capdevielle, G. Schatz, T. Thouw, and Others, *CORSIKA: A Monte Carlo code to simulate extensive air showers*, *FZKA* **6019** (1998).

[19] A. Ferrari, P. R. Sala, A. Fasso, and J. Ranft, *FLUKA: A multi-particle transport code (Program version 2005)*, *CERN-2005-010* (2005).

[20] K. Werner, F.-M. Liu, and T. Pierog, *Parton ladder splitting and the rapidity dependence of transverse momentum spectra in deuteron-gold collisions at the BNL Relativistic Heavy Ion Collider*, *Phys. Rev. C* **74** (2006) 044902.

[21] T. Pierog and K. Werner, *EPOS Model and Ultra High Energy Cosmic Rays*, *Nucl. Phys. B - Proc. Suppl.* **196** (2009) 102–105.

[22] D. Heck and R. Engel, *The EHISTORY and MUPROD Options of the Air Shower Simulation Program CORSIKA*, *KIT-SWP* **5** (2009).

[23] J. Matthews, *A Heitler model of extensive air showers*, *Astropart. Phys.* **22** (2005) 387–397.